Appl. Phys. B 72, 231–235 (2001) / Digital Object Identifier (DOI) 10.1007/s003400000244

Applied Physics B
Lasers
and Optics

Instabilities in laser-produced carbon plasma expanding in a nonuniform magnetic field

A. Neogi, R.K. Thareja*

Department of Physics, Indian Institute of Technology Kanpur, Kanpur 208016 (UP), India

Received: 26 August 1999/Revised version: 3 January 2000/Published online: 20 September 2000 –

Abstract. The laser-produced carbon plasma expanding in an ambient atmosphere in the presence of an inhomogeneous magnetic field has been studied by emission spectroscopy and fast photography. A double-peak structure is observed in the temporal profile of CII and CIII transition. A sudden increase in delay observed in the second peak when the plasma expands in the concave region of a magnetic field is attributed to Rayleigh–Taylor instability in a magnetic field. An estimate of the growth rate of the instability inferred using intensity and velocity profile of the expanding plasma is reported.

PACS: 52.25 Jm; 52.40 N; 94.30 Gm

The generation of a dense high-temperature plasma using lasers expanding across a magnetic field offers the possibilities of the investigation of instabilities. The physics of plasma flow across magnetic field lines regarding its collimation and stability properties is of particular relevance to the solar wind evolution [1], astrophysical jets [2], bipolar flows associated with young stellar objects [3], beam plasma heating [4], and cross field injection fueling of tokomak plasmas [5].

Plasma propagation across a magnetic field falls between two extreme limits. In the case of low-β (particle pressure/magnetic pressure) plasma that is in the nondiamagnetic limit, the magnetic field simply diffuses into the plasma and the plasma moves across the B field by $\boldsymbol{E} \times \boldsymbol{B}$ drift [6], whereas in case of high-β plasma, the diamagnetic limit, the plasma "punches" its way across the magnetic field giving rise to Rayleigh–Taylor instability [7, 8]. The Kelvin–Helmholz instability is another kind of magnetohydrodynamic instability which arises in a stratified fluid if the different layers are in relative motion [9]. Rayleigh–Taylor instability occurs when the density grows in the direction against the accelerating force [10]. For the motion of plasma (density $= \varrho_1$) in ambient gas (density $= \varrho_2$), the growth of the instability at the interface of the expanding plasma and the ambient gas can be expressed as [11]

$$\omega^2 = -kg\frac{(\varrho_1 - \varrho_2)}{(\varrho_1 + \varrho_2)} = -kg\alpha\,, \tag{1}$$

where g is the acceleration of the contact boundary. The plasma boundary is stable if $\omega^2 > 0$ whereas if $\omega^2 < 0$ the perturbation grows exponentially. The growth time of perturbation being

$$\tau = (kg\alpha)^{-\frac{1}{2}}\,. \tag{2}$$

In a magnetic field, a Rayleigh–Taylor instability occurs when a dense plasma (heavy fluid) is supported against gravity (light fluid) by the pressure of a magnetic field. An expanding plasma deforms the magnetic field resulting in magnetic forces that amplify the instability. In this paper, we report on the possible onset of Rayleigh–Taylor instability in laser-ablated plasma expanding in a concave magnetic field. A sudden enhancement in the delay of the second peak is observed in the temporal profile of CII transition $3d\ ^2D - 4f\ ^2F^0$ at 426.7 nm and CIII transition $3s\ ^3S - 3p\ ^3P^0$ at 465.0 nm. The enhancement is observed only in that region of the magnetic field where field lines are concave to the moving plasma, in accordance with the condition of occurence of Rayleigh–Taylor instability in a magnetic field.

1 Experimental setup

The experimental setup used in the present study is shown in Fig. 1. The field is maximum (3.5 KG) at the middle of the poles and decreases on either sides (along the x axis) whereas along the z direction it is minimum at the middle and maximum (5.1 KG) at the pole surface. A single pulse from a Nd:YAG laser (DCR-4G, Spectra Physics) delivering energy upto 1 J/pulse in fundamental mode ($\lambda = 1.06\,\mu$m) with full width at half maxima (FWHM) of 8 ns was focused on to the graphite target mounted in a vacuum chamber The diameter of the focused spot on the target was 240 μm. The target surface was flat and was translated after each shot in order

*Corresponding author. (E-mail: tharejark@hotmail.com)

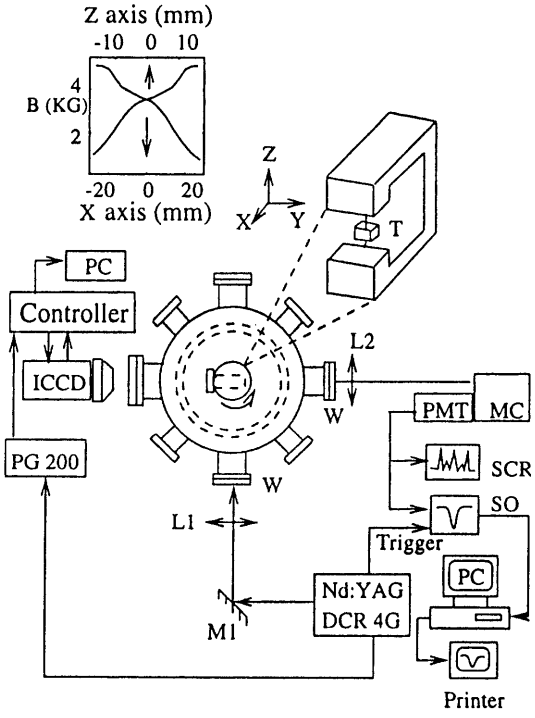

Fig. 1. Schematic of the experimental setup used. Position of the magnet and target is shown separately. T: target, MC: monochromator, SO: storage oscilloscope SCR: strip chart recorder, PG200: pulse generator, L1/L2: convex lens, ICCD: intensified charged coupled device. The magnetic field profile along z and x-axis is shown in the inset

to get fresh graphite surface every time. The plasma produced was imaged onto the slit of a monochromator (HRS2, Instruments S.A. Jobin Yvon) so as to have one to one correspondence with the plasma and its image. The output from the monochromator was detected with a photomultiplier tube (PMT) (IP28, Hamamatsu) and displayed onto the oscilloscope (TS-8123, Iwatsu). The two dimensional images of the expanding plasma were recorded by intensified charged coupled device camera system (ICCD-576G/2, Princeton Instrument). A 50 mm lens was used to image the plasma on to the detector surface. The detector consisted of microchannel plate (MCP) with spectral response in the region 200–820 nm and 384×576 CCD array. The digitized images were analysed using image processing software. Using the software one can obtain the total intensity, mean intensity, total area etc. from the total number of pixel covered by the plume.

2 Results and discussion

We have earlier reported the plasma expansion in vacuum, low pressure (5 mTorr and 100 mTorr) ambient atmosphere and in nonuniform magnetic field in vacuum using emission spectroscopy and fast photography [12–14]. The time-resolved emission spectra of carbon plasma were recorded at different distances away and parallel to the target surface by moving the monochromator in a plane perpendicular to the target surface. The temporal profile of CI transition $2p^3\,{}^3D^0 - 8f\ F(5/2)$ at 399.7 nm, CII transition $3d\ {}^2D - 4f\ {}^2F^0$ at 426.7 nm, CIII transition $3s\ {}^3S - 3p\ {}^3P^0$ at 465.0 nm, and CIV transition at $3s\ {}^2S - 3p\ {}^2P^0$ at 580.1 nm were recorded at various pressures of air. Each of these transitions is one of the strongest transitions in their respective ionic states. The emission lines are identified using the information available in the literature [15].

In case of vacuum, a single-peak structure is observed for all the species CI, CII, CIII, and CIV, whereas double-peak structure is observed for the case of plasma expanding in low-pressure ambient atmosphere (5 mTorr, 100 mTorr air) in CI, CII, and CIII transitions [12]. However, in the case of nonuniform magnetic field in vacuum, the temporal profile of the species showed multiple peaks and oscillations [13].

In the present reported experiment, in addition to the magnetic field, air at a pressure of 100 mTorr was introduced into the interaction chamber. We observed no multiple-peak structure and oscillations in the temporal profile. The nature of the temporal profile is dominated by the gas rather than by the magnetic field. That is the temporal profile at low-pressure air in magnetic field shows double-peak structure similar to the one observed earlier [12]. However, the presence of magnetic field increased the intensity of the temporal profile, and the onset distance of the occurence of the double peak compared to the case of no magnetic field (i.e. only gas). The increase in intensity is attributed to $q\boldsymbol{v} \times \boldsymbol{B}$ force acting on electrons and ions. The two forces being opposite in direction (for the electrons and ions), gives rise to surface current which is maximum at the plume boundary where the magnetic field is largest. This surface current due to finite resistivity of the plasma gives rise to Ohmic heating which attains the maximum value at the front edge of the expanding plume where the field is maximum.

A peculiar feature observed is the increase in delay of the second peak after a certain critical distance in the case of CIII and CII. Figure 2 shows the increase in delay of the second peak in the temporal profile of CIII transition on going from 12 mm to 14 mm from the target surface. In order to investigate the cause of the increased delay, the experiments were done in the following two configuration. First, keeping the target position fixed and monitoring the temporal profile of various species in the magnetic field. Since it was not possible to scan the whole region of the magnetic field due to the smaller dimensions of the plasma, a second alternative experi-

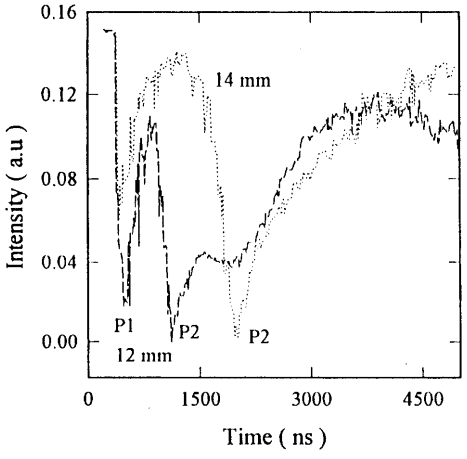

Fig. 2. The temporal profile of CIII transition at 12 mm (-) and at 14 mm (···). P1 and P2 are the first and second peak, respectively. A sudden delay in the second peak is observed on going from 12 to 14 mm in position T3 of the target position

ment was performed. Here the target was kept in six different positions in magnetic field at T1, T2, T3, T4, T5, and T6 as shown in Fig. 3 and the temporal profiles were monitored at various positions with respect to the target position. The delay of the second peak is plotted as a function of distance for different positions of the target in Fig. 4. It is observed that the temporal profile of CIII transitions show a sudden increase in delay of the second peak after a certain critical distance as for all positions of target except at T1. Position T2 shows the enhanced delay after 16 mm, position T3 after 12 mm, position T4 after 10 mm, position T5 after 12 mm, and position T6 after 16 mm, respectively. The position of the target and the corresponding onset point of increased delay, for example for position T2 it occurs at T2′ and similarly for others. as depicted in Fig. 3. Figure 5 shows the onset distance of the delayed second peak for different positions of the target in the magnetic field. Figures 3 and 5 show that as the target is moved towards the region of increasing magnetic field from T2 to T4 where the plasma first expands in the convex part of magnetic field and then concave region, the onset distance for the enhanced delay in the second peak decreases. For the positions T5 and T6, the plasma expands completely in the region where magnetic field lines are concave. The onset distance for the enhanced delay is observed to increase as the target is moved from position T5 to T6. It is important to note that the enhanced delay in the second peak occurs only at the latter half of the magnet where magnetic field lines are concave to the moving plasma. The enhanced delay never occurs at the first half of the magnet where field lines are convex to the moving plasma.

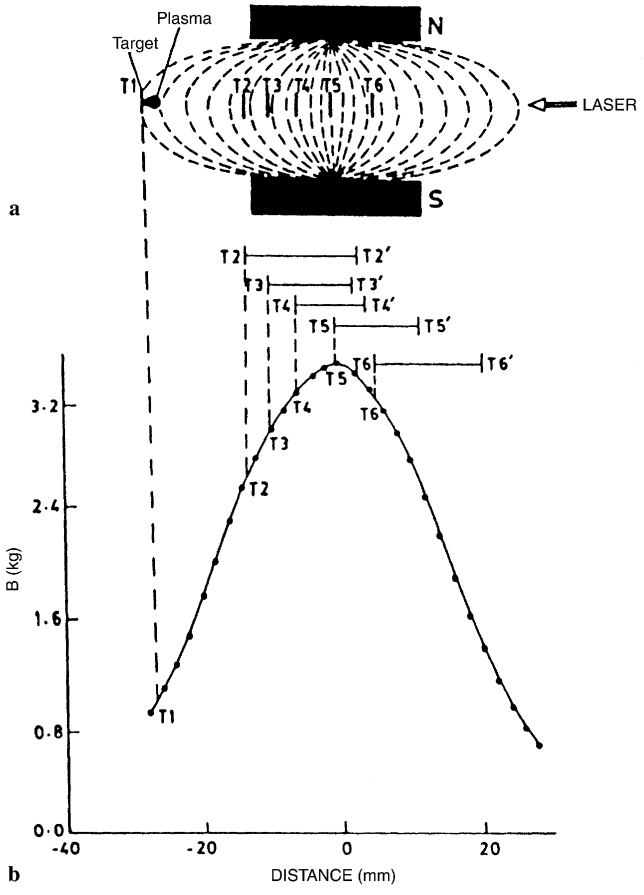

Fig. 3. a Different target positions with respective positions of the occurence of delayed second peak. **b** The measured variation of magnetic field strength in the direction of expanding plasma

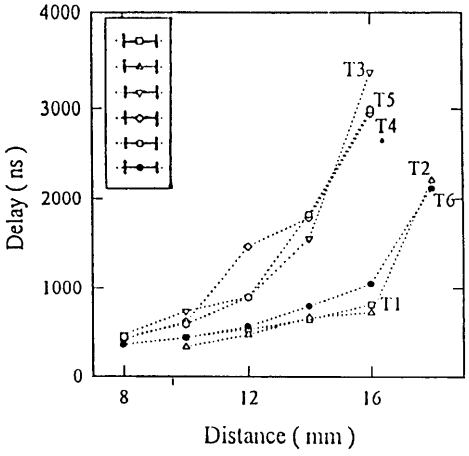

Fig. 4. Variation of delay of the second peak as a function of distance from the target position T1, T2, T3, T4, T5, and T6, respectively

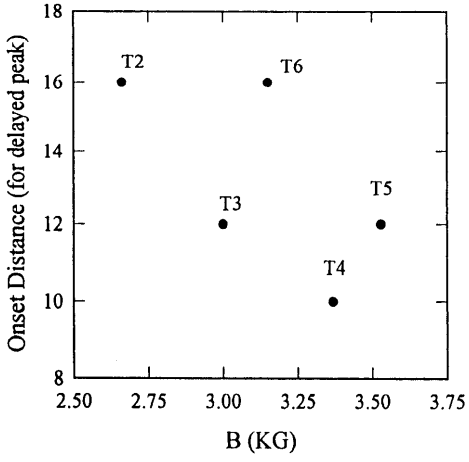

Fig. 5. The onset distance for the occurence of delayed second peak for different positions of the target in the magnetic field

Now we consider various possible processes responsible for the enhanced delay in the second peak. They may be recombination – three body recombination and radiative recombination, charge exchange, or magnetohydrodynamic instability. Let us investigate each of these processes in detail. The three-body recombination rate is given by $\alpha_c n_e{}^2 n_i$, whereas the radiative recombination rate is given by $\alpha_R n_e n_i$. α_c and α_R are the recombination coefficients for three-body recombination and radiative recombination, respectively. The calculation of recombination rate coefficient shows that radiative recombination is a dominant process close to the target surface, whereas three-body recombination process dominates a few mm away from the target surface. The three-body recombination coefficient is given by [16] in cm^6/s as

$$\alpha_c = 9.2 \times 10^{-27} Z^3 T_e{}^{-9/2} \ln\left[\sqrt{(Z^2+1)}\right], \qquad (3)$$

where Z is the charge number and T_e is the electron temperature in eV. In order to estimate α_c we measured the density of the plasma using the ICCD images and the Stark-broadened

profile of the transition [13]. The temperature was measured using the intensity ratio of various ionic lines and ICCD images [13, 14]. The measured temperature lies in the range 4–7 eV. The measured density is about $\approx 10^{17}$ /cm^3 at 4 mm from the target and decreases as the distance from the surface increases. Moreover, if recombination is the cause of the increased delay in the second peak the effect should have been more prominent for CI and CII transitions. However, the observations show that it is prominent for CIII and not for CI implying a low possibility of recombination. In the charge-exchange process an energetic ion or neutral captures either an ion or an electron and gets transfered to an energetic neutral. Calculations of charge-exchange cross section show that the possibility of charge exchange is much smaller. Moreover, the enhanced delay in the second peak is not observed for the neutrals suggesting a low probability of charge-exchange process. Let us now see the possibility of magnetohydrodynamic instabilities as the cause of the delayed second peak.

The condition for instability to occur is

$$-g\frac{n_1'}{n_1} > \frac{1}{4}k^2 v_1^2 , \tag{4}$$

where $n_1' = \frac{\partial n_1}{\partial x}$ and k is the wave vector It follows from (4), that the instability occurs when g and $\frac{n_1'}{n_1}$ have opposite sign. This is similar to the statement that light fluid is supporting the heavy fluid. The density fluctuations in the plasma near the interface boundary of plasma and magnetic field affect the structure of plasma profile. The first component penetrates into the field and the second component gets further delayed due to instability. If the lines of force are concave to the moving plasma, the centrifugal force experienced by plasma particles replaces the effect of g, and is in a direction opposite to the density gradient fulfilling the condition of Rayleigh–Taylor instability. If the lines of force are convex to the moving plasma, the plasma tends to be stabilized. In our case, the enhanced delay in the second peak occurs only in the region where magnetic field lines are concave to the moving plasma. It is obvious from Figs. 3 and 4 that as the target is moved to position T1, the plasma mostly travels through magnetic field lines that are convex to the moving plasma and hence the enhanced delay in second peak is not observed. Figure 6 shows a schematic diagram of an expanding plasma in a magnetic field. The $\boldsymbol{E} \times \boldsymbol{B}$ drift acting on the

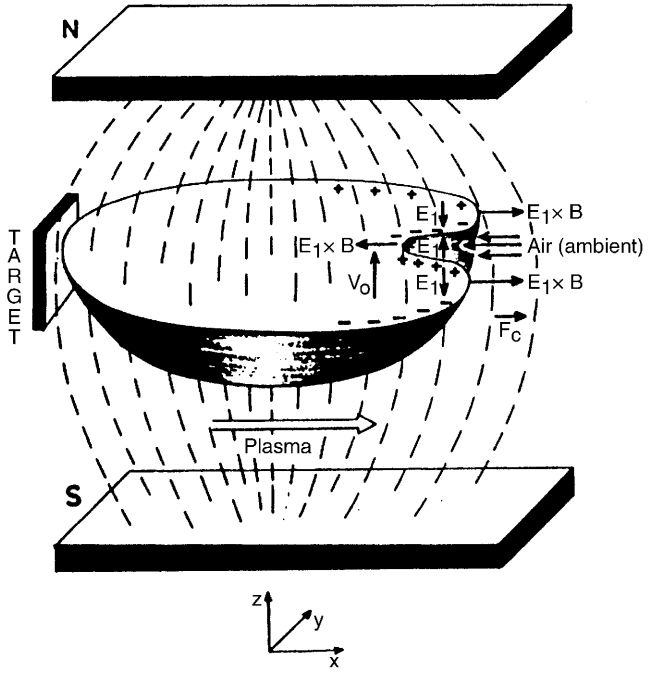

Fig. 6. A pictorial diagram showing the expansion of plasma in magnetic field in an ambient atmosphere

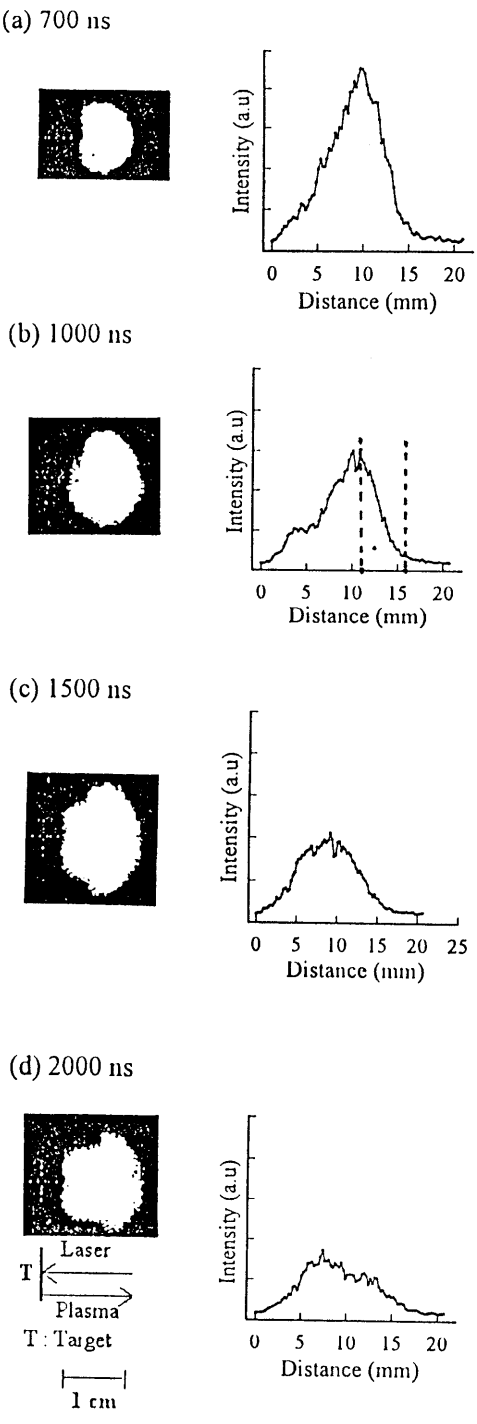

Fig. 7. The ICCD images and intensity profile of the plume at 700, 1000, 1500, and 2000 ns. The region in which density remains constant is within the *dotted line*

charged particles at the plasma boundary caused due to slight irregularities or perturbation are in the opposite direction giving rise to cracks or fissures, an outcome of Rayleigh–Taylor instability. The diffusion of air takes place through these fissures which results in the delayed component. Since charged particles play the major role at the surface the enhanced delay in the second peak is observed in the case of charged species only. An attempt is made to calculate the growth time of Rayleigh–Taylor instability from the intensity plots of ICCD photographs of the plume. The maximum growth rate of instability is given by

$$\gamma = \left(\frac{g_{\text{eff}}}{S}\right)^{\frac{1}{2}} , \tag{5}$$

where g_{eff} is the effective deceleration due to magnetic field and S is the density gradient scale length. Figure 7 gives ICCD images and the intensity plots at 700, 1000, 1500, and 2000 ns. These plots are of total emission intensity of all species in the plume. Comparison of intensity profiles at 700 ns and 1000 ns clearly shows the appearance of delay and occurence of cracks in the plume. A spectroscopic investigation reveals that plume predominantly has ionic species CII and CIII at this position [12]. The growth time of the instability which is the inverse of growth rate given by (5) can be estimated from the values of g_{eff} and S. The density gradient scale length at 1000 ns is estimated to be 5 mm from Fig. 7 (the length from the plasma boundary where density gradient remains constant, shown within the dotted line). Figure 8 gives the plot of velocity of the plasma front with time calculated from ICCD photographs. The slope of the velocity curve gives effective deceleration, g_{eff} which is estimated to be $0.554\,\text{cm}/\mu\text{s}^2$. The growth time of the Rayleigh–Taylor instability which is the inverse of growth rate comes out to be $0.95\,\mu$s (5). We have observed spectroscopically that enhanced delay in ionic component is most prominent at 1000 ns, in agreement with ICCD images. The calculated growth time of Rayleigh–Taylor instability using (5) (950 ns) matches the experimentally observed image of the plasma plume (at 1000 ns).

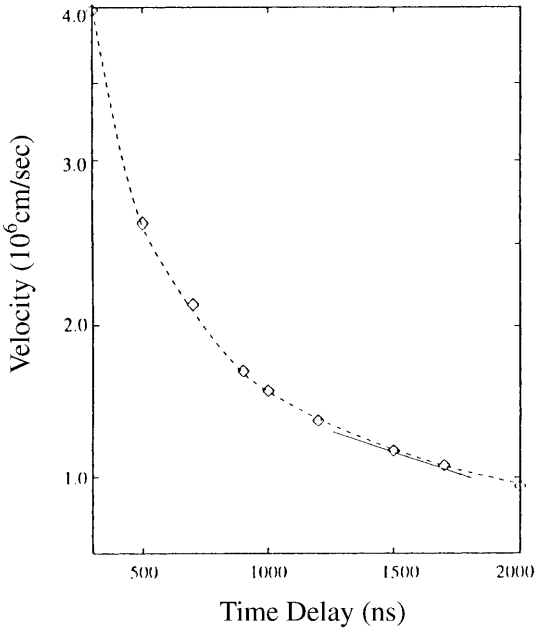

Fig. 8. The temporal variation of the velocity of the plume front calculated from ICCD photographs

The difference in the onset distance for the occurrence of enhanced delay in the second peak for different target positions viz. T3, T4, T5 in Fig. 3 can be explained using (5). The effective deceleration, g_{eff} controls the growth rate of Rayleigh–Taylor instability. The effective deceleration is caused by a $\boldsymbol{J} \times \boldsymbol{B}$ force. So the onset distance for enhanced delay is controlled by a $\boldsymbol{J} \times \boldsymbol{B}$ term integrated along a particular path. Qualitatively it can be said that average B is highest in the path T4 to T4′, so the integral of the $\boldsymbol{J} \times \boldsymbol{B}$ term brings required g_{eff} at a shortest distance (10 mm) followed by path T3 to T3′ (12 mm) and T5 to T5′ (12 mm) where the average B is lower than in the first case. As the average B of the path decreases, the path length increases such as in T6 to T6′ (16 mm) and T2 to T2′ (16 mm).

3 Conclusion

A sudden increase in the delay of the second peak in CIII transition is observed in the case of carbon plasma expanding in nonuniform magnetic field in 100-mTorr air. It is observed that the enhanced delay in the second peak occurs in that part of the magnetic field where magnetic field lines are concave to the moving plasma. Rayleigh–Taylor instability along with diffusion of air is attributed as the possible cause for the enhanced delay in the second peak. A rough estimate of the growth rate of Rayleigh–Taylor instability calculated from the intensity and velocity profile of ICCD photographs matches the experimental facts.

References

1. D.J. Southwood: Planet Space Sci. **16**, 587 (1968)
2. J.O. Burns, M.L. Norman, D.A. Clarke: Science **253**, 522 (1991)
3. R. Pudritz, M. Fich (Eds.): *Galactic and Extragalactic Star Formation*, NATO ASI Series C (Reidel, Dortrecht 1988)
4. E. Ott, W.M. Mannheimer: Nucl. Fusion **17**, 1057 (1977)
5. F.L. Waelbroeck, L. Chen: Phys. Fluids B **3**, 601 (1991); A. Bhattacharjee, R. Iacono, J.L. Milovich, C. Paramicas: Phys. Fluids B **1**, 2207 (1989)
6. J.W. Poukey: Phys. Fluids **10**, 2253 (1967)
7. B.H. Ripin, E.A. Melean, C.K. Manka, C. Pawley, J.A. Stamper, T.A. Peyser, A.N. Mostovych, J. Grun, A.B. Hassam, J. Huba: Phys. Rev. Lett. **59**, 2299 (1987)
8. J. Grun, M.E. Emery, C.K. Manka, T.N. Lee, E.A. Mclean, A.N. Mostovych, J.A. Stamper, S. Bodner, S.P. Obenschain, B.H. Ripin: Phys. Rev. Lett. **58**, 2672 (1987)
9. T.A. Peyser, C.K. Manka, B.H. Ripin, G. Ganguli: Phys. Fluids **4**, 2448 (1992)
10. H. Motz: *The Physics of Laser Fusion* (Academic Press, New York 1979)
11. Anan'in, ByKovski, Yu.V. Eremin, A.A. Zhuravlev, O.S. Lyubchenko, I.K. Navikov, S.P. Frolov: Sov. J. Quantum Electron. **21**, 787 (1991)
12. A. Neogi, A. Mishra, R.K. Thareja: J. Appl. Phys. **83**, 2831 (1998)
13. A. Neogi, R.K. Thareja: J. Appl. Phys. **85**, 1131 (1999)
14. A. Neogi, R.K. Thareja: Phys. Plasmas **6**, 365 (1999)
15. A.R. Striganov, N.S. Sventitskii: In *Tables of Spectral lines of Neutral and Ionised Atoms* (Plenum Press, New York 1968); W.L. Wiese, M.W. Smith, B.M. Glennon: *Atomic Transition Probabilities*, Vol 1, Natl. Bur. Stand. Ref. Data, Ser. Natl. Bur. Stand (U.S). Circ. No. 4 (U.S. GPO, Washington, DC 1966)
16. P.T. Rumbsy, J.M. Paul: Plasma Phys. **16**, 247 (1974)